American Mineralogist, Volume 81, pages 1350–1359, 1996

# Cation ordering in lead-molybdenum-vanadium oxychlorides

MARK D. WELCH, PAUL F. SCHOFIELD, GORDON CRESSEY, AND CHRIS J. STANLEY

Department of Mineralogy, Natural History Museum, Cromwell Road, London SW7 5BD, U.K.

## ABSTRACT

The crystal chemistry and structure of the layered lead oxychloride parkinsonite, ideally $Pb_7MoO_9Cl_2$, have been reevaluated in the light of TEM observations of natural and synthetic samples and the strong analogy with the D1*a* and $DO_{22}$ ordering patterns of Ni-Mo alloys. D1*a*-like superstructures occur in synthetic parkinsonite and V-bearing parkinsonite because of Pb-Mo and Pb-V ordering, with ordering stoichiometries $Pb_9Mo$ (10-site scheme) and $Pb_{18}V_2$ (20-site scheme). Natural parkinsonite orders on the $Pb_7Mo$ (8-site) or $Pb_{14}Mo_2$ (16-site) scheme. This ordering involves the formation of an incommensurate state that may be associated with a pseudohexagonal motif similar to the $DO_{22}$ superstructure in Ni-Mo alloys. It is our contention that X-ray methods usually miss important information about the superstructures in these minerals because of very high X-ray absorption. As a result, single-crystal structure refinements can lead to erroneous identification of the tetragonal or pseudotetragonal *I* subcell as the true unit cell. Transmission electron microscopy allows examination of extremely thin crystallites and observation of weak superstructure reflections. Crystal-chemical inferences about the structure and ordering behavior in these minerals are supported by EXAFS and XANES studies of a synthetic parkinsonite ordered on the 9:1 scheme, $Pb_9MoO_{11}Cl_2$, indicating that $Mo^{6+}$ may well be present in fivefold square-pyramidal coordination.

## INTRODUCTION

The structures of the layered lead oxychlorides are based on an alternation of litharge-like PbO layers and sheets of Cl atoms (Fig. 1). The main feature of interest is the wide diversity of elements that partially substitute for Pb: Si, P, As, V, Mo, and W (Aurivillius 1982). Charge balance and stable coordination are achieved by insertion of O atoms between Pb2 layers and creation of O vacancies within the PbO sheets. In kombatite, $Pb_{14}(VO_4)_2O_9Cl_4$ (Rouse et al. 1986; Cooper and Hawthorne 1994), each $V^{5+}$ is tetrahedrally coordinated, with the apical O atom providing bonding between adjacent Pb2 layers. Charge balance results in an O vacancy in the PbO layer. Kombatite and sahlinite, $Pb_{14}(AsO_4)_2O_9Cl_4$, both contain pentavalent cations and are isostructural (Rouse and Dunn 1985; Cooper and Hawthorne 1994). Asisite, ideally $Pb_7SiO_8Cl_2$ (Rouse et al. 1988), seems to be isostructural with parkinsonite (Symes et al. 1994). The latter authors give the formula of natural parkinsonite as $Pb_{6.34}Mo_{0.89}\square_{0.77}O_{8.02}Cl_{1.98}$ ($\square$ = cation vacancy). Recalculation of this formula for correct O stoichiometry for $Mo^{6+}$ substitution (O = 9 apfu), and excluding cation vacancies, gives $Pb_{7.13}Mo_{1.00}O_9Cl_{1.98}$, which is clearly compatible with the general $Pb_7X^{n+}O_{(6+0.5n)}Cl_2$ stoichiometry of kombatite, sahlinite, and asisite. Our reinterpretation of the parkinsonite structure precludes cation vacancies. Symes et al. (1994) found that, for natural parkinsonite, the best fit to the observed powder X-ray diffraction pattern is obtained when all Mo is only on sites within the Pb2 sublayer (Fig. 1). This is compatible with the preferential occurrence of V on analogous Pb2-like sites in kombatite (Cooper and Hawthorne 1994).

It seems that X-ray methods often miss the very weak superstructure reflections associated with Pb-X ordering, recording reflections only from the tetragonal subcell. It is this subcell (Fig. 1) that has been erroneously identified as the true unit cell in the case of parkinsonite (Symes et al. 1994). This may also be the case for the Si analog asisite (Rouse et al. 1988). The latter workers achieved an *R* index of 6.9% (weighted) without locating the Si positions. However, attempts to locate the Si atoms by a second difference synthesis failed. They attributed this failure to "the inconsiderable scattering power of ca. one Si atom per cell relative to that of the Pb atoms." The high mass-absorption coefficients for the layered lead oxychloride minerals (e.g., 840 $cm^{-1}$ for kombatite) can prevent the observation of the superstructure reflections. It was only by special sample preparation that the complex superstructure of kombatite was solved by Cooper and Hawthorne (1994).

In this paper, we present a reevaluation of the crystal chemistry of layered lead-molybdenum-vanadium oxychlorides primarily on the basis of electron diffraction data (TEM) and X-ray absorption spectroscopy (XAS) studies of Mo coordination in synthetic parkinsonite.

0003–004X/96/1112–1350$05.00

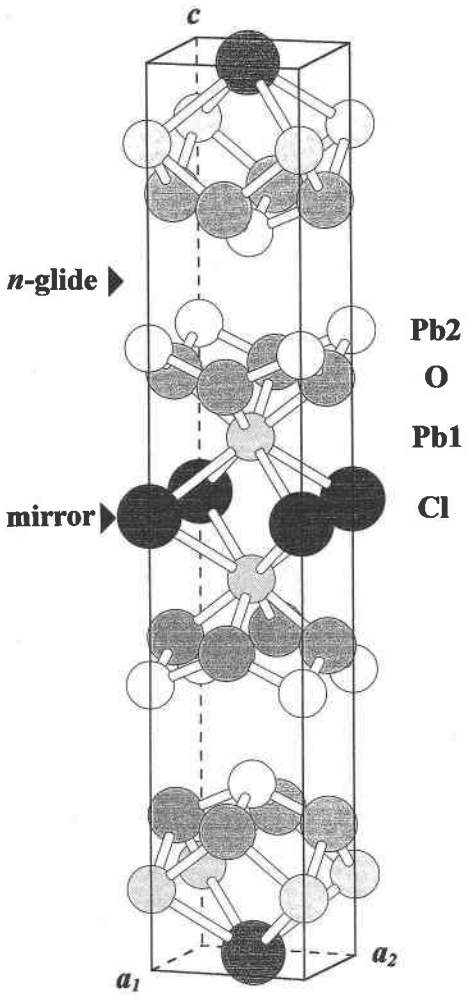


FIGURE 1. The subcell of parkinsonite ($a = b \approx 4$ Å, $c \approx 22.5$ Å). Pb1 sites are light gray, Pb2 sites are white, O sites are medium gray, and Cl sites are dark gray. The stacking module is Pb2-O-Pb1-Cl-Pb1-O-Pb2. The basic building block is the strongly bonded unit between *n* glides. The stacking direction is along *c* in the tetragonal varieties. The corresponding stacking orientation in monoclinic types is along *b*.

## EXPERIMENTAL PROCEDURES

### Synthesis

The procedure for synthesizing parkinsonite is described by Symes et al. (1994). The sample compositions are given in Table 1, and the bulk compositions are given in Table 2. The products were recovered from platinum crucibles as polycrystalline plugs of large (up to 3 mm diameter) interlocking plates of parkinsonite crystals. Bulk composition R1 is that of end-member parkinsonite. Although some sublimation of $PbCl_2$ was observed, this did not seem to have a serious effect on product stoichiometry or purity.

### X-ray and electron diffraction

Grains of parkinsonite (Symes et al. 1994; BM 1987,479), synthetic parkinsonite, V-bearing parkinsonite (BM 1994,55), and sahlinite (BM 1935,1131) were gently crushed in an agate pestle and mortar and sedimented onto holey carbon copper grids (Agar Products) from a suspension in clean absolute ethanol. The mounts were examined using a JEOL 100CX 100 kV transmission electron microscope fitted with a top-entry stage and a specimen holder that permitted ±10° tilt about two orthogonal axes. A 40 μm (0.45 $Å^{-1}$) objective aperture and a 200 μm condenser aperture were used. Larger condenser apertures resulted in the melting of crystallites. To increase the recorded intensities of very weak reflections present in some diffraction patterns and to obtain high-resolution images, we also examined the same samples at 200 kV using a JEOL 200CX microscope with a 50 μm objective aperture and a 200 μm condenser aperture. However, although the intensities of very weak reflections significantly increased, no high-resolution imaging was possible because of the opaque nature of the crystallites.

Single crystals of synthetic parkinsonite, parkinsonite (Symes et al. 1994), V-bearing parkinsonite, and sahlinite were examined by X-ray diffraction in Buerger precession geometry using Zr-filtered Mo*K*α radiation. Zero- and first-layer photographs were recorded; exposure times ranged from 1 to 8 d.

TABLE 1. Chemical compositions of parkinsonite samples

| | A | B | C | D | R1 | V-bearing parkinsonite |
|---|---|---|---|---|---|---|
| Pb | 85.6(0.67) | 84.49(0.42) | 83.57(0.39) | 83.37(0.39) | 83.35(0.51) | 84.48(0.41) |
| Mo | 3.28(0.13) | 4.14(0.07) | 4.76(0.11) | 5.01(0.07) | 5.00(0.27) | 2.14(0.02) |
| V | — | — | — | — | — | 0.95(0.02) |
| Cl | 3.93(0.07) | 4.09(0.06) | 4.23(0.07) | 4.25(0.06) | 4.38(0.36) | 4.11(0.12) |
| O | 7.37 | 7.68 | 7.88 | 7.98 | 7.95 | 7.11 |
| Total | 100.19 | 100.40 | 100.44 | 100.61 | 100.68 | 98.97 |
| | | | **Atoms pfu on the basis of (O + Cl) = 10** | | | |
| Pb | 7.23 | 6.85 | 6.59 | 6.50 | 6.49 | 7.07 |
| Mo | 0.60 | 0.73 | 0.81 | 0.84 | 0.84 | 0.39 |
| V | — | — | — | — | — | 0.32 |
| Cl | 1.94 | 1.94 | 1.95 | 1.94 | 1.99 | 2.01 |
| O | 8.06 | 8.06 | 8.05 | 8.06 | 8.01 | 8.03 |

*Note:* The weight-percent values are averages, and the numbers in parentheses are one standard deviation of the average ($n = 30$ analyses).

**TABLE 2.** Compositions of starting materials and synthetic parkinsonite products calculated on the basis of the three stoichiometries discussed in the text

| | A | B | C | D | R1 |
|---|---|---|---|---|---|
| | | | **Starting materials** | | |
| | | | $[\ldots O_8Cl_2]$ | | |
| Pb | 7.50 | 7.00 | 6.50 | 6.00 | 6.30 |
| Mo | 0.50 | 0.67 | 0.83 | 1.00 | 0.90 |
| | | | $[\ldots O_9Cl_2]$ | | |
| Pb | 8.33 | 7.77 | 7.22 | 6.67 | 7.00 |
| Mo | 0.56 | 0.74 | 0.92 | 1.11 | 1.00 |
| | | | $[\ldots O_{11}Cl_2]$ | | |
| Pb | 10.00 | 9.32 | 8.66 | 8.00 | 8.40 |
| Mo | 0.67 | 0.89 | 1.10 | 1.33 | 1.20 |
| | | | **Synthetic parkinsonite** | | |
| | | | $[\ldots O_8Cl_2]$ | | |
| Pb | 7.25 | 6.85 | 6.59 | 6.50 | 6.49 |
| Mo | 0.61 | 0.73 | 0.81 | 0.84 | 0.84 |
| | | | $[\ldots O_9Cl_2]$ | | |
| Pb | 8.05 | 7.61 | 7.32 | 7.22 | 7.21 |
| Mo | 0.68 | 0.81 | 0.90 | 0.93 | 0.93 |
| $\Delta_1$ | 5.56 | 2.82 | 0.35 | 0.91 | 0.9 |
| | | | $[\ldots O_{11}Cl_2]$ | | |
| Pb | 9.66 | 9.13 | 8.78 | 8.65 | 8.65 |
| Mo | 0.81 | 0.97 | 1.08 | 1.12 | 1.12 |
| $\Delta_2$ | 2.4 | 0.51 | 2.01 | 1.51 | 1.51 |

### Electron microprobe

Chemical analysis of parkinsonite and synthetic parkinsonite was performed using a Cameca SX50 electron microprobe operated at 20 kV and a current on the Faraday cage of 20 nA. Measured radiations were Pb$L\alpha$, Mo$L\alpha$, and Cl$K\alpha$. Standards were mendipite (Pb and Cl) and pure molybdenum and vanadium metals. Data were collected simultaneously using PET and LiF crystals and four spectrometers. Counting times were 30 s on the peak and 30 s for background.

### X-ray absorption spectroscopy

Samples were ground in an agate pestle and mortar and pressed into a thin plastic sample holder using Sellotape windows. Mo *K*-edge EXAFS spectra were recorded at the Synchrotron Radiation Source (SRS), Daresbury, U.K., operating in multibunch mode with an energy of 2 GeV and an average beam current of ~200 mA. Data for the standard material were collected in transmission mode, and for the synthetic parkinsonite in fluorescence mode, using a solid-state, 13-element Canberra detector on station 9.2 and using an Si(220) double-crystal monochromator. Data were calibrated by recording the spectrum of a 10 μm molybdenum metal foil and using the value 20002 eV for the position of the *K* edge.

X-ray absorption spectra were calibrated and background was subtracted using the SRS programs EXCAL and EXBACK, respectively. EXAFS analysis was performed using single-scattering rapid curved-wave theory (Gurman et al. 1984) and the SRS program EXCURV92 (Binsted et al. 1991) with ab initio phaseshifts calculated from χ-alpha potentials. The uncertainty associated with the coordination numbers and the Debye-Waller factors is ±20%, and the errors on the first-shell bond lengths are ±0.02 Å.

## RESULTS

### Chemistry

Chemical compositions of all parkinsonite samples studied by TEM are given in Table 1. Synthetic parkinsonite samples B and C contain small amounts (<5%) of blixite impurity, $Pb_2(O,OH)_2Cl$ (determined by X-ray diffraction and EMP analysis); synthetic parkinsonite samples D and R1 contain minor $Pb_2MoO_5$ (<5%). These minor amounts of impurities do not affect the conclusions of this study. Parkinsonite and V-bearing parkinsonite are free of impurities. Table 1 shows the average analysis ($n$ = 30) of each parkinsonite sample calculated for O + Cl = 10.

### Electron and X-ray diffraction observations

Here we describe selected-area electron diffraction patterns (SAEDPs) of parkinsonite, V-bearing parkinsonite, and synthetic parkinsonite and interpret them with reference to analogous observations on stoichiometrically related Ni-Mo alloys. SAEDPs are shown in Figure 2 and schematized in Figure 3.

**Synthetic parkinsonite.** In [001] SAEDPs of parkinsonite samples B, C, D, and R1, reflections of the type $h + k = 2n$ from the tetragonal $I$ subcell are intense. The forbidden $h + k = 2n + 1$ reflections (referred to substructure vectors) are slightly weaker. Long exposures (60–90 s) revealed that the diffraction patterns of all synthetic parkinsonite samples contain octets of very weak superstructure reflections with reciprocal lattice vectors $\frac{1}{5}[130]^*_{subcell}$. Exposure times of 7–8 d and very thin crystals (20 μm) were needed to observe these by X-ray precession photography, otherwise only reflections due to the tetragonal $I$ subcell were recorded. The aforementioned forbidden $h + k = 2n + 1$ reflections are not due to the substructure but result from superimposition of superstructure reflections at these points because of twinning (see below), and so there is no violation of systematic absences from the $I$ subcell. Interestingly, $Ni_4Mo$ alloy ordered on the D1$a$ scheme has an $hk0$ diffraction pattern (Okamoto and Thomas 1971, Fig. 4a; Das et al. 1973, Fig. 8) almost identical to synthetic parkinsonite B; the only difference is that the intensity of superstructure reflections (octets) relative to substructure reflections is greater for $Ni_4Mo$. Twinning results in superimposition of the two reciprocal lattices to give the octet superstructure reflection array. We propose a similar scheme for synthetic parkinsonite having the $Pb_9Mo$ ordering scheme. The different cation stoichiometries between these and the alloy result from the fact that in the latter Mo occupies all metal sheets, whereas in 9:1 synthetic parkinsonite only the Pb2 sublayers contain Mo. The stoichiometry of the (001) layer for $Ni_4Mo$ in the alloy and for Pb2 sublayers is $Pb_4Mo$ (Fig. 4).

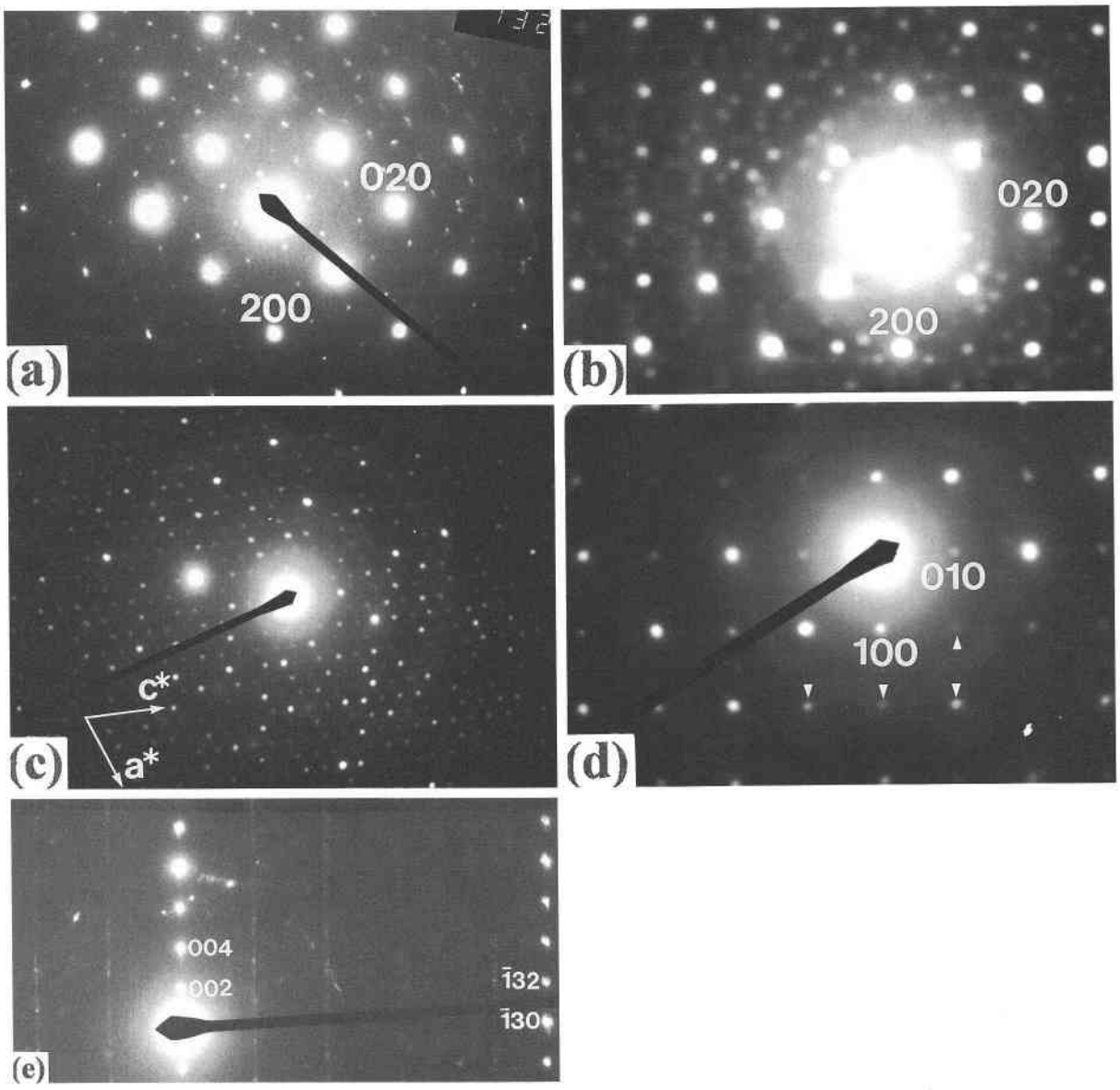


FIGURE 2. Parts **a**, **b**, and **d** are the [001] SAEDPs of V-bearing parkinsonite, synthetic parkinsonite ($Pb_9MoO_9Cl_2$), and parkinsonite, respectively. Part **c** is a [010] SAEDP of sahlinite. All have the electron-beam direction normal to PbO sheets in their respective structures. The substructure-superstructure relations are shown in Figure 3. In the SAEDP of parkinsonite (**d**), arrows indicate some of the reflections about which the ring of diffuse intensity with six weak satellite reflections is most easily seen. Part **e** is the $c^*$-[$\bar{1}$30]* SAEDP of V-bearing parkinsonite, showing weak lines of modulated intensity parallel to $c^*$. These lines occur at intervals of $\frac{1}{5}$[130]*, corresponding to the positions of superstructure reflections observed in [001] SAEDPs.

Okamoto and Thomas (1971) obtained bright- and dark-field images of D1$a$ $Ni_4Mo$ that showed a very fine-scale mottled microstructure of domains 10–20 Å in diameter; these domains are microtwins. We expended considerable effort trying to obtain high-resolution images, but even the thinnest crystallites and broken edges were opaque and showed no microstructural details, even at 200 kV.

**V-bearing parkinsonite.** The [001] SAEDPs of V-bearing parkinsonite have quartets of $\frac{1}{5}$[130]* superstructure reflections. It is evident (Fig. 2) that each quartet is one of a pair that defines the octets of superstructure reflections observed in synthetic parkinsonite (see above). In some SAEDPs, quartets are perfect squares, whereas others have a small (<5°) monoclinic distortion (e.g., Fig. 2a). We suggest that crystallites with square quartets are Mo rich, and those with nonsquare quartets are V rich. Both represent ordering on the 9:1 (or 18:2) scheme. A

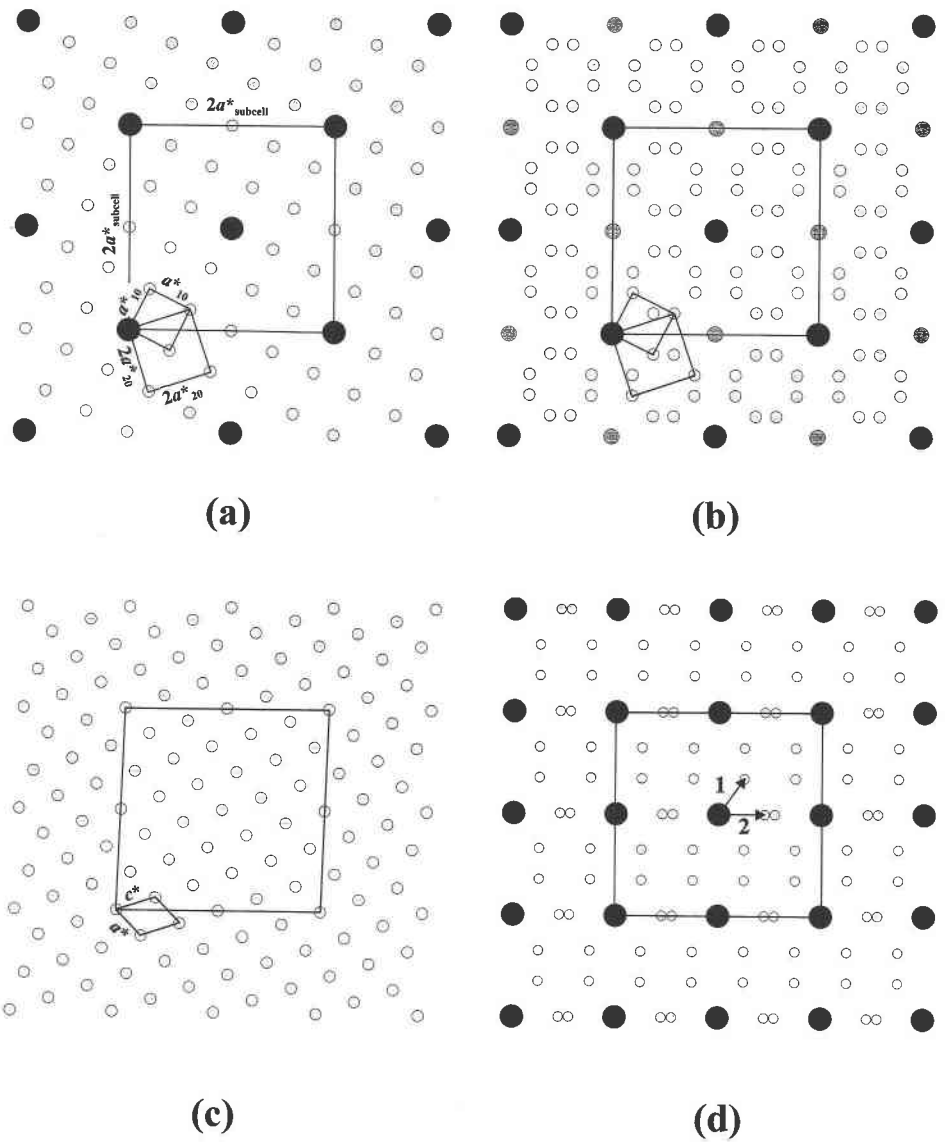


**FIGURE 3.** Schematic illustrations of the SAEDPs of Figure 2. (**a**) V-bearing parkinsonite, (**b**) synthetic parkinsonite, (**c**) sahlinite, and (**d**) parkinsonite. Relationships between reciprocal substructures and superstructures are indicated. The small light-gray spots are superstructure reflections, and the large black spots are substructure reflections. Note that for synthetic parkinsonite the moderately strong forbidden $h + k = 2n + 1$ reflections are shown as medium-gray spots. The subcell of sahlinite has a small monoclinic distortion. In **d** the vectors 1 and 2 are of unequal length but are both ~0.1 $Å^{-1}$ long.

slight monoclinic distortion of the square motif is to be expected by comparison with kombatite, in which the pairs of $VO_4$ tetrahedra all have the same oblique orientation and lead to motif point symmetry 2. The moderately intense forbidden $h + k = 2n + 1$ reflections observed in synthetic parkinsonite SAEDPs are of the same intensity as other weak superstructure reflections in V-bearing parkinsonite. This is consistent with the untwinned nature of the superstructure in the latter and also supports the idea that the $h + k = 2n + 1$ reflections in synthetic parkinsonite are enhanced by twinning. The superstructure reflections of synthetic parkinsonite and V-bearing parkinsonite are so weak that no information is available from these for imaging.

**Parkinsonite.** The [001] SAEDPs of natural parkinsonite show an array of strong reflections that are based on a square corresponding to [100]* of the substructure; forbidden $h + k = 2n + 1$ reflections occur. Centered on each of these reflections is a "ring" of diffuse intensity associated with a pseudohexagonal array of extremely weak satellite reflections at ~0.11 $Å^{-1}$ from the main reflection (Figs. 2d and 3d). The satellite reflections appear streaked and occur in three pairs, with each member of a pair sharing a distinct streaking direction: [210], [$2\bar{1}0$], or

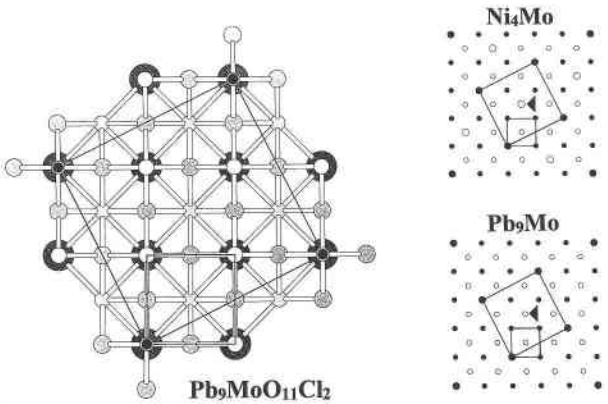


FIGURE 4. Proposed $Pb_9MoO_{11}Cl_2$ supercell for synthetic parkinsonite samples based on the D1*a* ordering scheme of $Ni_4Mo$. Pb1 sites are light gray, Pb2 sites are white, O sites are medium gray, and Cl sites are dark gray. Mo sites are shown as small black circles at the corners of the supercell square. To the right are the ordering patterns of D1*a* $Ni_4Mo$ and the analogous $Pb_9MoO_{11}Cl_2$ parkinsonite, in which the black and white circles correspond to cation sites in two layers (Pb1 and Pb2 for $Pb_9MoO_{11}Cl_2$ parkinsonite); larger circles are atoms of the minor element. Note that the $Pb_9Mo$ scheme has only Mo at the Pb2 site. Superstructure-substructure relations are indicated in all three diagrams.

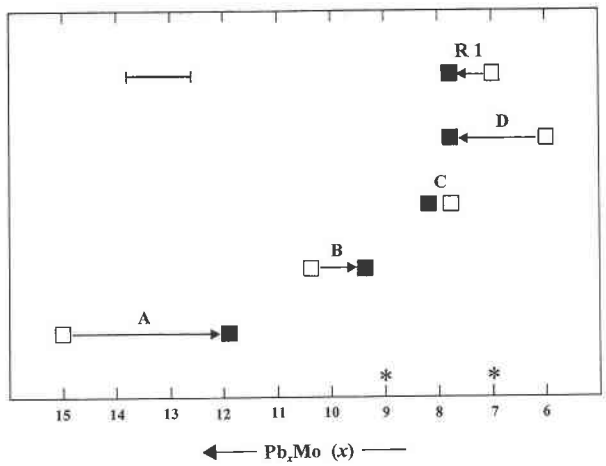


FIGURE 5. Compositions of starting materials (open squares) and synthetic parkinsonite sample (solid squares), expressed as Pb/Mo (see text). The $Pb_9Mo$ and $Pb_7Mo$ ordering stoichiometries are indicated by asterisks. The analytical uncertainty is indicated by the error bar at the upper left.

[010]. Strikingly similar diffraction behavior was observed in Fe-bearing åkermanite by Seifert et al. (1987, Fig. 5D), in which it is associated with the incommensurate-to-commensurate transition. An origin for the rings of diffuse intensity was not suggested by Seifert et al. (1987). However, in the case of parkinsonite, we suggest a possible origin in the Discussion section.

In addition to the intralayer superstructure reflections associated with cation ordering, there are diffuse and modulated variations in diffraction intensity perpendicular to the layers. Figure 2e is a $c^*$-[$\bar{1}$30]* section (referred to substructure vectors) of V-bearing parkinsonite; the lines of weak intensity are associated with all *hk*0 superstructure reflections and suggest that an additional multiple-*c* superstructure exists. A similar $c^*$-modulated variation in the intensities of superstructure reflections has been observed in penfieldite, $Pb_2Cl_3OH$ (Merlino et al. 1995). However, in V-bearing parkinsonite the $c^*$ superstructure reflections are absent from rows of substructure reflections, which is not the case in penfieldite. In synthetic parkinsonite, all ⅕[130]* superstructure reflections are streaked along $c^*$ and do not seem to be associated with a multiple-*c* superstructure; however, they could be due to polytypic stacking disorder.

The SAEDPs of synthetic parkinsonite samples B, C, D, and R1 indicate that these structures order on a D1*a*-like scheme, which, given that Mo occurs only at Pb2 sites, implies $Pb_9Mo$ stoichiometry. Our proposed $Pb_9MoO_{11}Cl_2$ supercell ($a = b \approx 8.95$ Å, $c \approx 22.5$ Å) is shown in Figure 4 and is based on the D1*a* atomic ordering pattern of $Ni_4Mo$. This figure also shows a comparison between the sheet motifs in $Pb_9MoO_{11}Cl_2$ parkinsonite and $Ni_4Mo$. The point symmetry of the two-dimensional supercell sheet motif is 4, whereas that of the subcell is 4*mm*. In Table 2 we attempt to evaluate the microprobe data (Table 1) with regard to this ordering stoichiometry. In both super- and subcells all Cl sites are fully occupied. Consequently, charge balance must be achieved by inserting O atoms into the space between adjacent Pb2 layers (Fig. 1) or removing O atoms from the PbO sheet, as in kombatite. This should be borne in mind when recalculating analyses to different formulas (see below). Table 2 shows the analytical data recalculated to three distinct anion stoichiometries: (1) $[Pb,Mo,\square]_xO_8Cl_2$ (cf. Symes et al. 1994); (2) $[Pb,Mo]_yO_9Cl_2$ (to test for $Pb_7Mo$ ordering); (3) $[Pb,Mo]_zO_{11}Cl_2$ (to test for $Pb_9Mo$ ordering). This involves recalculating Pb and Mo to 18, 20, and 24 negative charges, respectively. Note that the Cl contents remain unchanged, as required by the structural models. As an indication of the extent of agreement with the ideal $Pb_7Mo$ and $Pb_9Mo$ stoichiometries, we define the indices $\Delta_1$ and $\Delta_2$ as $\Delta_1 = |\Sigma \text{ cations} - 8| + |\text{Pb/Mo} - 7|$ and $\Delta_2 = |\Sigma \text{ cations} - 10| + |\text{Pb/Mo} - 9|$. Taking into account analytical errors of Pb and Mo, values of $\Delta < 2$ indicate close approach to a given ordering stoichiometry. The results are presented in Table 2 and Figure 5. It is evident that for parkinsonite samples B, C, D, and R1 there is convergence on Pb/Mo of about 8–9. This accords well with the TEM observations that samples B, C, D, and R1 are ordered on the $Pb_9Mo$ scheme. Deviations from ideal $Pb_9Mo$ stoichiometry are due to a combination of analytical uncertainty and genuine compositional differences. Nonetheless, the electron diffraction data indicate that the synthetic parkinsonite samples are composed primarily of sheets ordered on the $Pb_9Mo$ scheme. Parkinsonite A is

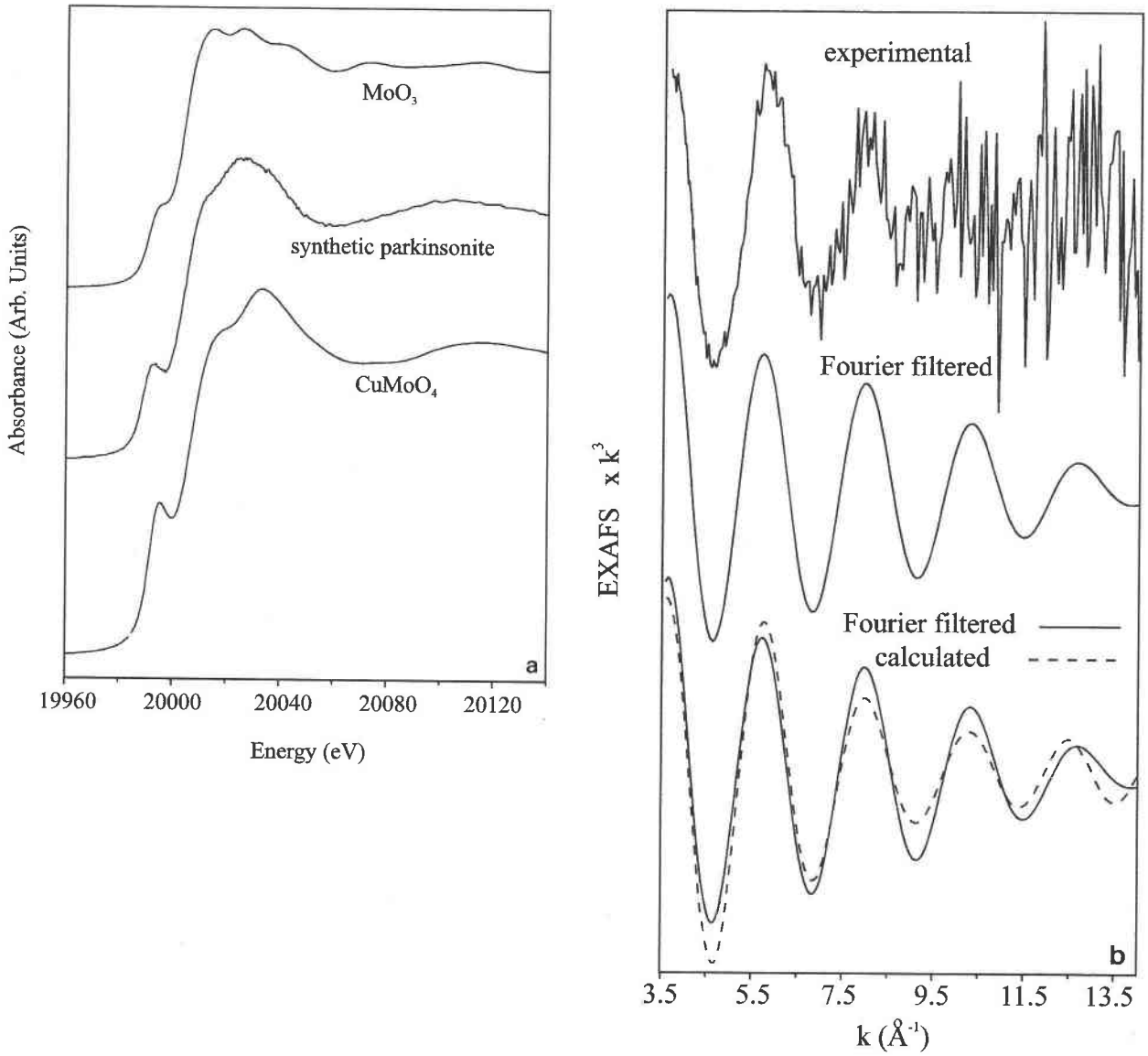


FIGURE 6. (**a**) Mo *K*-edge XANES spectra of $MoO_3$ (top), parkinsonite B (middle), and $CuMoO_4$ (bottom). (**b**) Mo *K*-edge EXAFS of synthetic parkinsonite B. The background-subtracted raw data are shown at the top, the back-transformed EXAFS filtered from the first peak in the Fourier transform of the experimental EXAFS is in the middle, and the calculated fit (dashed line), for a model involving four short Mo-O bonds and one long Mo-O bond, to the Fourier-filtered EXAFS (solid line) is at the bottom.

substantially displaced from bulk composition A and coexists with blixite impurity. Although no superstructure reflections were found, it is possible that Parkinsonite A is an intercalation of litharge-like PbO and minor $Pb_9Mo$-ordered layers.

### X-ray absorption spectroscopy

All parkinsonite samples were tested with a strong REE permanent magnet; they were all nonmagnetic. This suggests that Mo may be present as $Mo^{6+}$ rather than $Mo^{5+}$ (magnetic). Charge balancing of $Mo^{6+}$ must involve the addition of an O atom to the positively charged PbO structural unit. In kombatite, tetrahedral coordination of $V^{5+}$ is achieved by insertion of an apical O atom between Pb2 layers and the creation of an O vacancy within the same PbO sheet. As a logical next step, we assumed that this O site is not vacant in parkinsonite. This implies that $Mo^{6+}$ has fivefold-coordinated square-pyramidal configuration. Furthermore, to avoid prohibitively high incident bond valence at O atoms, the $MoO_5$ groups are likely to be isolated rather than polymerized (e.g., as $Mo_2O_9$ groups). We used XANES and EXAFS to try to resolve these possibilities.

The preedge and XANES regions of $MoO_3$, synthetic parkinsonite, and $CuMoO_4$ are shown in Figure 6a. The positions of the absorption edges are within a few elec-

tron volts (the Mo $K$ edge of parkinsonite is ~1 eV higher than that of $MoO_3$ and ~3.5 eV lower than that of $CuMoO_4$), confirming that Mo is in the hexavalent state in parkinsonite. The shapes of the preedge and XANES regions can give information about the bonding and polyhedral geometry of the target cation. The preedge feature for $Mo^{6+}$ cations was associated with the 1s-4d bound-state transition by Cramer et al. (1978). In a manner analogous to that of $Ti^{4+}$, the intensity of the preedge feature also increases as the coordination geometry changes from octahedral coordination to pentahedral coordination to tetrahedral coordination, although distortions from holosymmetric octahedral symmetry also enhance this feature. Furthermore, Cramer et al. (1978) stated that the intensity of this preedge feature varies directly with the number of terminal, nonbridging Mo=O double bonds, increasing in intensity as the number of these Mo=O bonds increase, and has been used to identify the structures of $Mo^{6+}$ species in solution (Yokoi et al. 1987, 1993).

The preedge feature of $MoO_3$ is present as a shoulder on the main absorption edge and is induced by the large degree of distortion that exists in the $MoO_6$ octahedron. The same feature is very well developed in the spectrum of $CuMoO_4$, in which the $Mo^{6+}$ cation is present in tetrahedral coordination; indeed, the intensity is ~50% of the edge step. The preedge peak for synthetic parkinsonite is also well developed, but the intensity is only ~38% of the edge step, and the peak is also separated from the edge by 2.8 eV more than the corresponding feature in $CuMoO_4$. Although it is not possible to use the preedge feature as a definitive indicator of exact ligand structure, we can confidently eliminate the possibility of tetrahedral coordination for the $Mo^{6+}$ cation in parkinsonite.

To a lesser extent, the shape of the XANES features may also be used to interpret the coordination geometry of the $Mo^{6+}$ cation (Evans and Mosselmans 1991). Tetrahedral and octahedral species generally produce two distinct maxima directly after the edge, with an energy separation on the order of 20 eV. For a fivefold-coordinated species, these two peaks are less distinct. The lower energy maximum is present as a shoulder on the second maximum, and the separation is dependent on the size of the basal angle (Evans and Mosselmans 1991). In this case, the XANES region appears similar to that of a square-pyramidal species with a basal angle in the region of 110°.

The requirement to extract only nearest-neighbor information from the rather noisy raw EXAFS signal encouraged us to analyze back-transformed EXAFS filtered from the Fourier transform of the raw data. The results are summarized in Table 3 and Figure 6b. The reliability of the ab initio phase shifts was checked by comparing EXAFS-derived bond lengths with the crystallographic data of Abrahams et al. (1968) for $CuMoO_4$. These data are shown in Table 3 and are an excellent match. It is also important to note that, from the crystal-chemical arguments discussed above, certain constraints can legitimately be placed on the modeling of the EXAFS spectrum: The coordination environment should conform to the symmetry suggested by both the crystal-chemical reasoning and the electron diffraction results.

**TABLE 3.** Data from EXAFS analysis of $CuMoO_4$ and synthetic parkinsonite

| Atom type | N | Bond length (Å) | $2\sigma^2$ (Å$^2$) | $R$ factor |
|---|---|---|---|---|
| O | 4.01 | 1.76 | 0.009 | 15.03 |
| O | 4 | 1.772 | | |
| **Synthetic parkinsonite, fixed N, 1 shell** | | | | |
| O | 4 | 1.82 | 0.019 | 38.33 |
| O | 5 | 1.83 | 0.022 | 40.09 |
| O | 6 | 1.83 | 0.028 | 43.20 |
| **Iterated N, 1 shell** | | | | |
| O | 4.46 | 1.83 | 0.022 | 40.08 |
| **Fixed N, 2 shells, fivefold coordinated** | | | | |
| O | 4 | 1.83 | 0.015 | 36.07 |
| O | 1 | 2.03 | 0.010 | |
| O | 1 | 1.79 | 0.004 | 33.03 |
| O | 4 | 1.89 | 0.026 | |
| **Sixfold coordinated** | | | | |
| O | 4 | 1.82 | 0.015 | 35.96 |
| O | 2 | 2.02 | 0.020 | |
| O | 2 | 1.81 | 0.009 | 34.54 |
| O | 4 | 1.94 | 0.037 | |
| O | 3 | 1.82 | 0.013 | 35.03 |
| O | 3 | 1.99 | 0.031 | |
| **Fixed N, 3 shells** | | | | |
| O | 2 | 1.79 | 0.005 | 31.84 |
| O | 2 | 1.92 | 0.007 | |
| O | 2 | 2.08 | 0.027 | |
| O | 1 | 1.78 | 0.003 | 31.39 |
| O | 4 | 1.89 | 0.021 | |
| O | 1 | 2.14 | 0.025 | |

*Note:* The uncertainties for the iterated coordination number (N), bond length, and Debye-Waller factors ($2\sigma^2$) are ±20%, ±20%, and ±0.02 Å, respectively. The $R$ factor is a measure of goodness-of-fit between the calculated EXAFS and the Fourier-filtered EXAFS. $CuMoO_4$, Abrahams et al. (1968).

Analysis assuming a single shell of coordinating O ligands of fixed number is relatively uninformative. The fit to the data for each single-shell model is poor; indeed, the EXAFS is fitted closely only up to a $k$ value of ~8 Å$^{-1}$, whereas two-shell models fit the EXAFS closely for $k > 11$ Å$^{-1}$. From these single-shell models, however, we can discount tetrahedral coordination of $Mo^{6+}$ because we might expect fit parameters and statistics similar to those derived for $CuMoO_4$. If the coordination number within the single-shell model is not fixed, a value of 4.46 results. EXAFS inherently underestimates the value of the coordination number, implying that, in this case, tetrahedral coordination is unlikely and so a coordination number of 5 rather than 6 is the most favorable option. In a two-shell model with a coordination number of 5, the best model involved square-pyramidal geometry and not trigonal-bipyramidal geometry. Indeed, the model assuming one short bond and four long bonds is clearly preferable to the model with four short bonds and one long bond, which produces both a larger $R$ factor and an unexpectedly long Mo=O bond (Cramer et al. 1978).

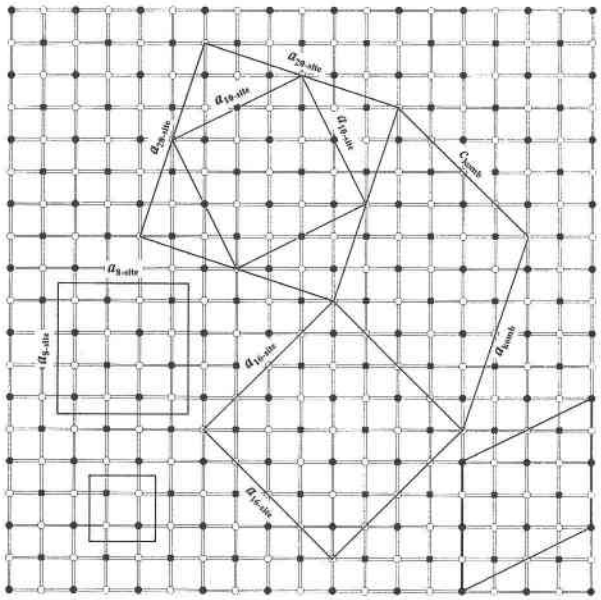

**FIGURE 7.** Geometrical relationships among various ordering motifs relevant to lead-molybdenum-vanadium-arsenic oxychlorides. The supercells are superimposed on a litharge PbO sheet (black circles are Pb, Mo, V, and As; white circles are O). Shown are the subcell motif (bottom left), the 10- and 20-site square motifs of synthetic and V-bearing parkinsonite, the monoclinic 16-site motif of kombatite, token 8- and 16-site square motifs, and a monoclinic 8-site motif (lower right) that may be the basis of the pseudohexagonal ordering pattern of parkinsonite.

Models involving two shells and octahedral geometry all produce poorer fits to the EXAFS data, with higher $R$ factors than that for square-pyramidal geometry involving a short Mo=O bond. When the octahedral models are split into three shells, the $R$ factors are not reduced significantly from that of the best square-pyramidal model and only reflect the increased number of variable parameters. The data for these models certainly do not suggest an improvement; they also conflict with the crystal-chemical reasoning and lead to unlikely bond lengths.

Although these XAS results cannot categorically prove that the proposed coordination environment for the $Mo^{6+}$ cation is correct, they do suggest that square-pyramidal geometry is not unrealistic. Indeed, although such a polyhedral environment is very unusual for $Mo^{6+}$, the XAS results do suggest that square-pyramidal geometry, with one short Mo=O bond and four longer Mo-O bonds, is the most favorable coordination state for Mo in parkinsonite.

## DISCUSSION

The TEM observations and chemical data indicate that lead-molybdenum-vanadium oxychlorides order on 10-site ($Pb_9Mo$), 16-site ($Pb_{14}Mo_2$, $Pb_{14}V_2$), 8-site ($Pb_7Mo$), and, possibly, 20-site ($Pb_{18}V_2$) schemes. EXAFS does not discount the possibility that $Mo^{6+}$ is in square-pyramidal coordination, as required by the structural model for parkinsonite. The major ordering schemes of the lead-molybdenum-vanadium-arsenic layered oxychlorides are shown in Figure 7. The kombatite (sahlinite) motif is very different from the two other square 16-site motifs. Synthetic parkinsonite orders on the $Pb_9Mo$ scheme and has a single motif because the square-pyramidal $MoO_5$ groups are not locally associated. In contrast, the $VO_4$ tetrahedra in kombatite are paired. This precludes the smaller 10-site motif, which would give $Pb_8V_2$, the wrong cation stoichiometry. In fact, the smallest possible motif for V-bearing parkinsonite is the 20-site motif. The overall stoichiometries for the 16- and 20-site schemes are $Pb_{14}X_2^{n+}O_{12+n}Cl_4$ and $Pb_{18}X_2^{n+}O_{16+n}Cl_4$, respectively.

As noted in the Results section, the SAEDPs of parkinsonite show rings of diffuse intensity, with radius of ~0.11 $Å^{-1}$, around all substructure reflections. Within each ring there are six local intensity maxima in a pseudohexagonal array, as shown in Figure 3d. We can attempt an interpretation of this diffraction behavior on the basis of crystal-chemical reasoning and a comparison with the ordering behavior of Ni-Mo alloys. If we assume that bond-valence constraints preclude adjacency of $Mo^{6+}$ ions, then the smallest motifs consistent with $Pb_7Mo$ stoichiometry are those shown in Figure 7. The superstructure in the lower-right corner of Figure 7 is pseudohexagonal and closely related to the $DO_{22}$ superstructure observed in Ni-Mo alloys (Okamoto and Thomas 1971); another supercell is square with $a = 2a_{subcell}$. Okamoto and Thomas (1971) showed how the various alloy superstructures can be produced one from another by the periodic stacking of {210} layers of pure Mo atoms. Intermediate structures are composed of identically ordered domains bounded by {210} antiphase boundaries (APBs). Nonconservative APBs have the structure of a different ordering scheme. The reader is referred to Okamoto and Thomas (1971) for a detailed description of the transformations. Streaking of some satellite reflections along [210] or $[2\bar{1}0]$ may be due to periodic {210} APBs. A correlated domain microstructure, in which domains ordered on the pseudohexagonal ($DO_{22}$-like) motif are separated by periodic APBs with $\lambda \approx 9.3$ Å, is a possibility. Such a modulation is incommensurate with respect to this pseudohexagonal superstructure. This scheme also explains satellites streaked along [010] because periodic (010) APBs are a consequence of the periodic {210} APBs. The presence of these satellites suggests that parkinsonite has a significant degree of long-range Pb-Mo ordering. Parkinsonite is probably either $Pb_7MoO_9Cl_2$ (8 site) or $Pb_{14}Mo_2O_{18}Cl_4$ (16 site), and SAEDPs indicate that the ordering scheme may involve a microstructure in which domains with a pseudohexagonal (8-site) motif are related by periodic APBs, leading to an incommensurate microdomain state analogous to the behavior of some Ni-Mo alloys.

Chemical compositions of V-bearing parkinsonite suggest solid solution between Mo and V. However, if it is assumed that V occurs as pairs of $VO_4$ tetrahedra, as in kombatite, then the dispositions of Mo and V in their

respective ordering schemes must be very different. The major difference is that the stoichiometry of the unit mesh for Mo is $Pb_9Mo$ (10 site), whereas that for V is $Pb_{18}V_2$ (20 site). The question then arises as to whether or not these two schemes can occur within a single PbO sheet as ordered domains of pure $Pb_9Mo$ and $Pb_{18}V_2$; or is there true solid solution (Mo and V mixing)? Much circumstantial evidence points to a high degree of cation order within the PbO sheets in parkinsonite, V-bearing parkinsonite, sahlinite, and kombatite. First, parkinsonite and kombatite have simple formulas that can be easily related to cation-ordering schemes within PbO sheets. Similarly, chemical analysis indicates that asisite has a 9:1 ordering scheme. The key point here is that the mineral formula is the stoichiometry of the ordering scheme. Second, Pb-Mo order is present in synthetic parkinsonite that grows in seconds; it may not be possible to quench in primary disorder. This is also true of rapidly quenched $Ni_4Mo$ alloy. These observations and the foregoing reasoning suggest that individual PbO sheets have either the 10-site or 20-site scheme. If this is the case, the sheets are chemically distinct and the mineral is an intercalation of Pb-Mo layers with 9:1 ordering on the 10-site scheme and Pb-V layers with 18:2 ordering on the 20-site scheme. Therefore, the apparent solid solution in V-bearing parkinsonite may be spurious and due to fine-scale mixtures of chemically distinct layers. The X-ray excitation volume associated with the microprobe electron beam penetrates to a depth of approximately 4–5 μm and passes through many PbO layers (7000–9000), therefore giving a bulk analysis that suggests solid solution where none exists. Because stacking disorder may be common in these minerals (for example, it occurs in synthetic parkinsonite and V-bearing parkinsonite), it is likely to be difficult to prove that there are such fine-scale mixtures.

## Acknowledgments

We thank Andrew Putnis and Ian Marshall for giving M.D.W. access to the transmission electron microscope at the Department of Earth Sciences, Cambridge University. Barbara Cressey is also thanked for allowing M.D.W. to use the TEM at the Department of Geology, Southampton University. J. Frederick W. Mosselmans is thanked for his assistance associated with the XAS analysis, and we thank Gary Jones (NHM) for his alchemical skill in synthesizing parkinsonite. M.D.W. thanks the NHM for a senior research fellowship. We thank Robert Symes and Alan Criddle for introducing us to these fascinating minerals.

## References cited

Abrahams, S.C., Bernstein, J.L., and Jamieson, P.B. (1968) Crystal structure of the transition-metal molybdates and tungstates: IV. Paramagnetic $CuMoO_4$. Journal of Chemical Physics, 48, 2619–2629.

Aurivillius, B. (1982) On the crystal structures of a number of non-stoichiometric mixed lead oxide halides composed of PbO-like blocks and single halogen layers. Chemica Scripta, 19, 97–107.

Binsted, N., Campbell, J.W., Gurman, S.J., and Stephenson, P.C. (1991) SERC Daresbury Laboratory program EXCURV92, Daresbury, U.K.

Cooper, M., and Hawthorne, F.C. (1994) The crystal structure of kombatite, $Pb_{14}(VO_4)_2O_9Cl_4$, a complex heteropolyhedral sheet mineral. American Mineralogist, 79, 550–554.

Cramer, S.P., Hodgson, K.O., Gillum, W.O., and Mortenson, L.E. (1978) The molybdenum site of nitrogenase: Preliminary structural evidence from X-ray absorption spectroscopy. Journal of the American Chemical Society, 100, 3398–3407.

Das, S.K., Okamoto, P.R., Fisher, M.J., and Thomas, G. (1973) Short-range order in Ni-Mo, Au-Cr and Au-Mn alloys. Acta Metallurgica, 21, 913–928.

Evans, J., and Mosselmans, J.F.W. (1991) Study of the XANES modeling of molybdenum compounds. Journal of the American Chemical Society, 113, 3737–3742.

Gurman, S.J., Binsted, N., and Ross, I. (1984) Single scattering curved wave theory. Journal of Physics C: Solid State Physics, 19, 1845–1861.

Merlino, S., Pasero, M., Perchiazzi, N., and Gianfagna, A. (1995) X-ray and electron diffraction study of Penfieldite: Average structure and multiple cells. Mineralogical Magazine, 59, 341–348.

Okamoto, P.R., and Thomas, G. (1971) On short-range order and microdomains in the $Ni_4Mo$ system. Acta Metallurgica, 19, 825–841.

Rouse, R.C., and Dunn, P.J. (1985) A re-examination of sahlinite from Långbon, Sweden. Neues Jahrbuch für Mineralogie Monatshefte, 127–131.

Rouse, R.C., Dunn, P.J., and Innes, J. (1986) Kombatite, the vanadium analogue of sahlinite, from the Kombat mine, South West Africa. Neues Jahrbuch für Mineralogie Monatshefte, 519–522.

Rouse, R.C., Peacor, D.R., Dunn, P.J., Criddle, A.J., Stanley, C.J., and Innes, J. (1988) Asisite, a silicon-bearing lead oxychloride from the Kombat mine, South West Africa (Namibia). American Mineralogist, 73, 643–650.

Seifert, F., Czank, M., Simons, B., and Schmahl, W. (1987) A commensurate-incommensurate phase transition in iron-bearing åkermanites. Physics and Chemistry of Minerals, 14, 26–35.

Symes, R.F., Cressey, G., Criddle, A.J., Stanley, C.J., Francis, J., and Jones, G.C. (1994) Parkinsonite $(Pb,Mo,\square)_8O_8Cl_2$, a new mineral from Merehead Quarry, Somerset. Mineralogical Magazine, 58, 59–68.

Yokoi, K., Matsubayashi, N., Miyanaga, T., Watanabe, I., Murata, K., and Ikeda, S. (1987) Studies on the structure of cationic dimer of molybdenum(VI) in acidic solution by XANES and EXAFS. Chemistry Letters, 1453–1456.

Yokoi, K., Matsubayashi, N., Miyanaga, T., Watanabe, I., and Ikeda, S. (1993) Studies on the structure of molybdenum(VI) in acidic solution by XANES and EXAFS. Polyhedron, 12, 911–914.

Manuscript received September 7, 1995
Manuscript accepted June 28, 1996